Chapter 2

A NEW EXPERIMENTAL TECHNIQUE FOR STUDYING STRONG ELECTRIC FIELD EFFECTS ON LIQUID CRYSTALS

2.1 Introduction

As described in Chapter 1, most of the anisotropic physical properties of nematic liquid crystals are of the nature of second rank tensors. When an electric field ($\vec{E}$) is applied at an angle θ with respect to the director ($\hat{n}$), due to this tensorial nature, the free energy density can be written as (see Figure 2.1)

$$F^E = -\frac{1}{8\pi}\epsilon_{\parallel}E^2\cos^2\theta - \frac{1}{8\pi}\epsilon_{\perp}E^2\sin^2\theta \tag{2.1}$$

where $\epsilon_{\parallel}$ and $\epsilon_{\perp}$ are the principal dielectric constants. Equation 2.1 can be written as

$$F^E = -\frac{1}{8\pi}\epsilon_a(\hat{n}.\vec{E})^2 - \frac{1}{8\pi}\epsilon_{\perp}E^2. \tag{2.2}$$

When the electric field is low $\epsilon_{\parallel}$ and $\epsilon_{\perp}$ remain practically unchanged. Accordingly, the second term in Equation 2.2 adds a constant to the free energy and thus can be ignored. For a nematic with positive dielectric anisotropy it can be seen from Equation 2.2 that the free energy density is minimised when the director aligns parallel to the electric field while for a material with negative dielectric anisotropy the minimum occurs when the director is perpendicular to the field. The orientational order parameter is given as (as described in Chapter 1)

$$S = \frac{\epsilon_{\parallel} - \epsilon_{\perp}}{\Delta\epsilon_o} \tag{2.3}$$

where $\Delta\epsilon_o$ is the dielectric anisotropy for the fully aligned state. Thus the director reorients to be parallel (or perpendicular) to the electric field at constant S (as $\epsilon_{\parallel}$ and $\epsilon_{\perp}$ remain unchanged in the presence of a small field).

In the following, we restrict our discussion to materials with positive dielectric anisotropy. When an electric field is applied, parallel to the director, from Equation 2.1 we obtain

$$F^E = -\frac{1}{8\pi}\epsilon_{\parallel}E^2. \tag{2.4}$$

Here it is seen that the free energy density is minimised if $\epsilon_{\parallel}$ itself increases with electric field. As a result, $\epsilon_{\perp}$ decreases. This in turn leads to an increase in the orientational order parameter, S (Equation 2.3). Expressing $\epsilon_{\parallel}$ in terms of S we get

$$\epsilon_{\parallel} = \bar{\epsilon} + \frac{2}{3}\Delta\epsilon_o S \tag{2.5}$$

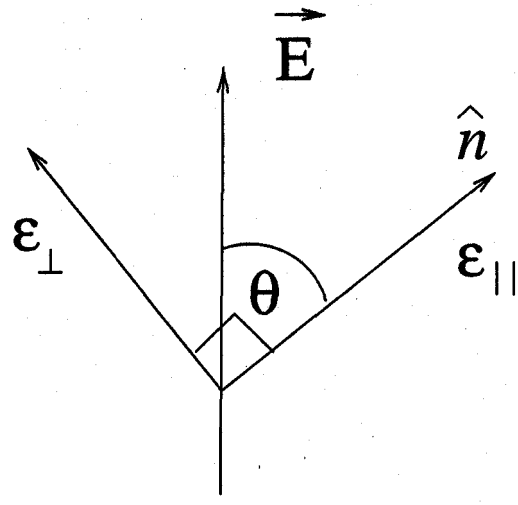

Figure 2.1: Diagram showing the direction of the electric field with respect to the director A.

where $\bar{\epsilon} = (\epsilon_{||} + 2\epsilon_{\perp})/3$ is the average dielectric constant. In the presence of a strong electric field Equation 2.4 reduces to

$$F^E = -\frac{\Delta\epsilon_o S E^2}{12\pi}, \tag{2.6}$$

ignoring the term containing $\bar{\epsilon}$ assuming that it remains unchanged.

Thus in the presence of a strong electric field a term linear in S and quadratic in E, has to be included in the free energy expression. As can be seen from Equation 2.6 the free energy can be lowered if S takes a higher value in the presence of the field. Thus the application of a strong electric field to a nematic liquid crystal leads to an enhancement of the orientational order parameter [21].

In addition to the above effect, it was shown by de Gennes that the thermal fluctuations of the director are suppressed under the action of a magnetic field (or equally an electric field), thus leading to an enhancement of the order parameter that is *linearly* dependent on the magnitude of the applied field [1, 22]. This effect will be discussed in greater detail in Chapter 5.

When a field is applied to the *isotropic* phase, it induces an orientational order in the medium. This leads to a weak induced anisotropy in all the physical properties, for eg to birefringence. When a magnetic field is applied the induced birefringence is called the Cotton-Moutton effect, and when an electric field is applied it is called the Kerr effect. In this *paranematic* phase the field induced order is uniaxial. Thus the higher temperature paranematic phase and the lower temperature nematic phase have the same symmetry, hence ruling out the possibility of a second order phase transition between them. As such, there can be either a jump in the order parameter at the transition point in a first order transition or a continuous evolution of the order parameter. It is expected that the jump in the order parameter at the transition point decreases as the field is increased, and goes to zero at a critical field. Further the critical temperature will be higher than the field free transition temperature.

The phenomenon is similar to the classic liquid-gas transition under the application of pressure. There have been a number of theoretical calculations on the detailed phase diagrams in the presence of a field in the framework of the Landau theory [23, 24, 25]. There are also some molecular models that discuss this problem [26, 27, 28].

Using a magnetic field in such studies makes the interpretation of the data simpler as the

problems arising from ionic, electrode and electrohydrodynamic effects are absent [29, 30]. For a field to shift the transition temperature by a measurable amount, the energy (F^E or F^m, the free energy density due to the presence of an electric or magnetic field), should be comparable with the intermolecular interactions responsible for the long range orientational order i.e. with the thermal energy, k_BT. A typical nematic has a volume diamagnetic anisotropy of 10^{-7} cgs units and the *molecular* diamagnetic anisotropy χ_m is given by

$$\chi_m = \frac{\chi_a}{N} \tag{2.7}$$

where N is the number of molecules per unit volume.

$$N = \frac{N_A \rho}{M} \tag{2.8}$$

where ρ is the density of the medium $N_A = 6.02 \times 10^{23}$ /mole is the Avogadro number and M is the molecular weight. The magnetic energy per molecule is given by

$$\mathcal{E}_m = \frac{-\chi_m H^2}{2}. \tag{2.9}$$

Assuming $M = 300$, $\rho = 1$ gm/cc, T = 300K and $k_B = 1.38 \times 10^{-16}$ ergs/K $\chi_m \sim 10^{-29}$ cgs units, for the field energy to be equal to the thermal energy, H should be $\sim 10^7$ gauss. So far only magnetic fields of strength $\sim 10^5$ gauss have been applied to thermotropic liquid crystalline systems producing very small shifts in the nematic-isotropic transition temperature (~ 6 mk)

This problem can be overcome if larger rod-like objects are used to form the nematic phase, so that the molecular diamagnetic anisotropy of the constituent objects of the system under study is increased. This has been achieved in some specific lyotropic systems. Tang and Fraden [32] were able to observe a magnetic field induced isotropic-nematic phase transition at a constant temperature, in an aqueous colloidal suspension of fd virus, which exhibits the nematic phase at high concentrations of the virus in the absence of the field. The virus has a large length to diameter ratio of ~ 140, whereas thermotropic liquid crystals have molecules whose length to diameter ratio is ~ 4. This in turn increases the molecular diamagnetic anisotropy by ~ 25 times in the former case. In addition these particles have a molecular weight of 1.6×10^7, leading to a χ_m of $\sim 10^{-23}$ cgs units. Thus the magnetic field required to have a measurable effect on the system reduces to $\sim 10^4$ gauss. To observe the induced order the authors measured the induced birefringence as a function of field. For concentrations in a narrow range, in which the sample was in the isotropic phase but close to the nematic phase, they observed a nonlinear induced birefringence as a function of applied magnetic field ($\sim 15 \times 10^4$ gauss). As they were studying a multicomponent lyotropic system the phase transition involves two order parameters i.e. one characterising the orientational order and the other, the particle concentration. The dynamics of these two order parameters further complicates the analysis of the experimental results.

Coming back to thermotropic liquid crystal systems, the dielectric anisotropy can be much larger (~ 10) than the diamagnetic anisotropy. Making a similar calculation as described above, but now replacing χ_a by $\epsilon_a/4\pi$ and H by E one finds that for the electric field required for the electric field energy ($\mathcal{E}_E$) to be of the order of the thermal energy, E should be $\sim 10^5$ V/cm (~ 300 esu). This electric field is practically attainable in the laboratory.

However when such a large electric field is applied, the sample gets locally heated due to the dissipation of energy arising from the ionic flow in the sample. This effect can be reduced

if one uses a high frequency AC field. Even if the frequency of the AC field is large enough to reduce the ionic effects,the sample heats up due to dielectric relaxation processes. As one wants to bring down E (the field required for the field energy to be comparable to the thermal energy) it would be desirable to use liquid crystals with a large ϵ_a. This is possible if there is a large dipole moment along the long axis of the molecule. However in this case the relaxation of the orientational polarisation, due to the molecular rotation around the short axis occurs at quite low frequencies ($\sim 10^6$ hertz) because of the orientational order of the nematic phase [4]. Near the relaxation frequency, dielectric losses lead to a substantial local heating of the sample. The dielectric heating effect has been studied in detail by Schadt both in nematics [33] and smectics [34].

There have been many attempts to study the electric field induced effects on the orientational order in nematic liquid crystals. Helfrich [35] was the first to demonstrate that by applying large AC or DC electric fields a positive shift in the nematic-isotropic transition temperature (T_{NI}) occurs. He maintained a temperature gradient across the length of the experimental cell thus allowing for the observation of the nematic-isotropic phase boundary. When a sufficiently strong voltage was applied the boundary shifted towards the higher temperature part of the cell. Viewing the samples in transmitted light he was able to measure the shift in the boundary and hence the shift in the transition temperature. These observations had to be made immediately after the field was applied before the sample heated up.

Nicastro and Keyes [36] measured the induced birefringence under the application of a DC electric field in materials with positive and negative dielectric anisotropies. They used two iconel strips as electrodes as well as spacers for controlling the thickness of the cell. They measured the optical path difference induced by the electric field with the light propagating perpendicular to the field direction. They did not measure the heating that occurred due to the electric field and hence their results have only a qualitative significance. Also, as mentioned earlier, other problems arise due to the DC electric field, like double layer formation and injection of charges at the electrodes leading to electrohydrodynamic effects. Thus it is better to use an AC voltage than a DC voltage in such experiments.

Recently Lelidis and Durand [37, 38] could study the electric field phase diagram quantitatively by applying bursts of pulsed AC electric fields with a few positive and negative half period square waves of high enough frequency ($\sim$ 100 KHz) to avoid ionic flow effects. The pulses lasted for $\tau \sim 10$ to 100 μs with a time interval T $\sim$ 10 s. With $\tau/T < 10^{-5}$ they argued that the heating was negligible. They used an optical technique to monitor the order parameter of the sample and fitted their data to a simple Landau theory. To decrease the uncertainty in the measurement of the increase in the order parameter($\delta(\Delta S)$) to $\pm$0.002, they had to accumulate the data over 2^8 pulses. Thus to obtain one data point it took about forty minutes. They have also verified the theoretical prediction [39] that an external field can induce a nematic phase with a large orientational order in materials which undergo a direct smectic A to isotropic phase transition [40]. More recently using this technique they have optically measured the dynamics of the orientational order parameter in 5CB, induced by an electric field [41]

Rjumstev et *al* [42, 43] have also used pulses to study the influence of high electric fields on the nematic-isotropic phase transition. They used a 2 ms wide pulse with a special shape : an exponentially rising front edge and a sharp rear edge. They made optical measurements using a photodetector whose output was connected to an oscilloscope. The voltage rise at the front edge of the pulse resulted in the appearance of maxima and minima in the light flux, corresponding to changes in the phase difference between the interfering ordinary and extraordinary waves. They have reported field induced birefringence in both positive and negative dielec-

tric anisotropy materials at temperatures above T_{NI}. They could determine the shift in the phase transition temperature due to the application of a strong field in some positive dielectric anisotropy materials.

In the last two experiments the authors have used short pulsed electric fields so that the sample does not heat up during the measurement. We have taken a different approach to the problem. It is clear that the local heating will not be a problem if the local temperature of the sample can be measured. We have developed such a technique which will be described below.

2.2 Experimental Techniques

The experimental liquid crystal cells consist of two parallel conducting plates. Strong electric field effects are measured in cells which have an active area of $\sim 1\ cm^2$ and thickness ~ 10 to 50 pm. Obviously the thickness limits the maximum field that can be applied to the sample. If the local temperature of the cell has to be accurately measured the sensor has to be in as close a proximity as possible to the active area. The best result is achieved if the sensor is directly below the active area. Also the sensor should be electrically insulated from the electrode which is used to apply the electric field to the cell.

Certain metals are known to have high temperature coefficients of resistance, for egchromium, nickel and platinum. By vacuum evaporating one of these metals on a glass plate, one can use this film as the temperature sensor. In principle it would be ideal to use platinum as the temperature sensor as it is a highly stable metal and has a linear temperature coefficient over a large temperature range. But platinum cannot be easily vacuum coated on glass as it has a very high melting point. We initially tried using chromium, as it adheres strongly to glass. However it easily oxidises forming a semiconductor which has a negative temperature coefficient of resistance. Also the temperature coefficient was quite low and further the resistance of the coating was not reproducible when the plate was thermally cycled. Hence we have used nickel coating .as the in *situ* sample temperature sensor.

2.2.1 Construction of the Cell

The nickel film which is coated on a glass plate is patterned using a photolithographic technique. To do this, a thin film of photoresist is applied over the nickel coated plate. It is cured in the oven at 80°C for ~ 10 min. The mask (negative) of the required pattern is placed in as close a proximity as possible on the plate, and the plate is exposed to UV light for ~0.5 min. Then the plate is developed for ~ 1 min. This plate is again cured in the oven at 100°C for ~ 2 Hours. The unexposed part of nickel is etched using a solution of lgm ferricyanide in 50 ml water. The plate is then washed with water, and the remaining photo resist is removed with chloroform.

A zigzag pattern which has a strip width $\sim 200\mu m$ and a total length ~ 5 cm is used to obtain a resistance ~ 180 to 450 Ω at room temperature, the value depending on the thickness of the nickel coating. The pattern is confined to a circular region of 0.5 cm diameter as shown in Figure 2.2, and rectangular extensions on both sides with an area of $\sim 1\ cm^2$ each for making electrical connections. The width of the rectangular strips has been chosen to be much larger than that of the zigzag pattern to reduce their resistance to, $\sim$ a few ohms. The resistivity of nickel is $10.3 \times 10^{-6}\ \Omega$ cm at T =273K. From the above numbers the thickness of the film can be estimated to be ~ 0.1 pm. The resistance varies by ~ 1 to $2\ \Omega/K$. It is covered by an insulating layer of SiO or SiO_2 on which an aluminium electrode is deposited in vacuum. The required type of pattern for the electrode is again etched in the aluminium coating using a photolithographic technique. The etchant for aluminium is a solution of 3-4 pellets of NaOH

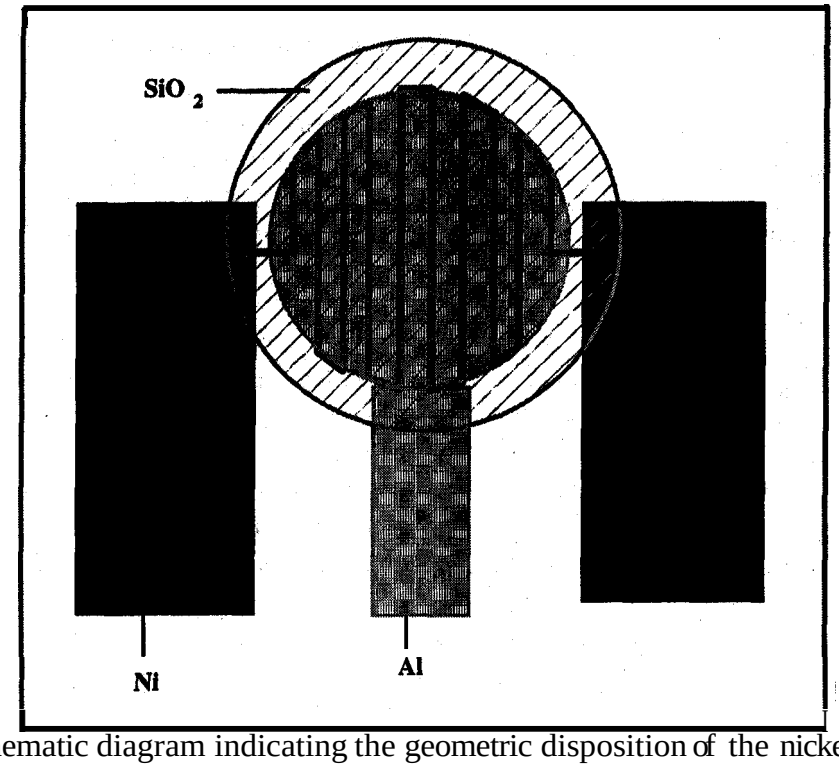

Figure 2.2: Schematic diagram indicating the geometric disposition of the nickel thermometer, SiO_2 insulator and the aluminium electrode on the lower plate of the cell.

or KOH and 0.5 gram of potassium ferricyanide dissolved in 50 ml water. In our experiments we have used two different types of configurations for the aluminium electrode. Initially we used only a circular electrode with a rectangular extension for electrical connections (see Figure 2.2). But in this case there will be a field gradient around the edge of the electrode. To reduce these edge effects we have redesigned the electrode to include a guard ring (see Figure 2.3). In the latter, the region over which the electrical and optical measurements are made will have a reasonably uniform field. This will also minimise the temperature gradients near the edge of the electrode. For the counter electrode we have used a single circular electrode with a rectangular extension etched either in an ITO or aluminium-coated glass plate (Figure 2.4).

The electrodes were treated with ODSE (octadecyltriethylsilane) before assembling the cell to get homeotropic alignment of the nematic liquid crystal. Electrical connections were made by using conducting silver paste to attach teflon coated wires to the cell.

The gap between the two plates is fixed by mylar spacers and is typically between 10 to 25 μm. Care was taken to make sure that the adhesive (used to seal the cell) and the spacer were not in the active area. The cell thickness is measured by using an optical interference technique. The white light reflected normally from the two surfaces bounding the air gap corresponding to the cell thickness is made to fall on a constant deviation spectroscope (Adam and Hilger Ltd.). A spectrum with alternate dark and bright fringes is seen due to interference of light reflected from the two surfaces of the cell forming the air film, adjacent to the aluminium coating. The cell thickness is calculated using the expression

$$d = \frac{\lambda_m \times \lambda_n}{\lambda_m - \lambda_n} \times \frac{n - m}{2} \qquad (2.10)$$

where λ_m and λ_n are the wavelengths corresponding to the m^{th} and n^{th} dark fringes respectively. As the transparent region is very limited in some cases it was not possible to use the above method to measure the thickness. Also the reflection from the aluminium coating reduced the

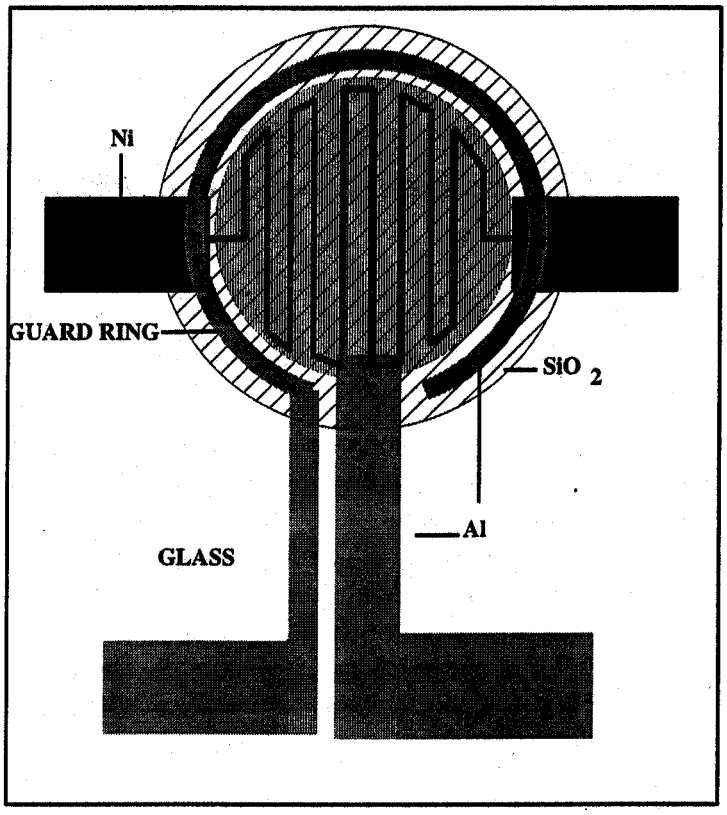

Figure 2.3: Schematic diagram of the improved configuration indicating the geometric disposition of the nickel thermometer, SiO_2 insulator and the aluminium electrode on the lower plate of the cell. This is the configuration used for later experiments. It includes a guard ring.

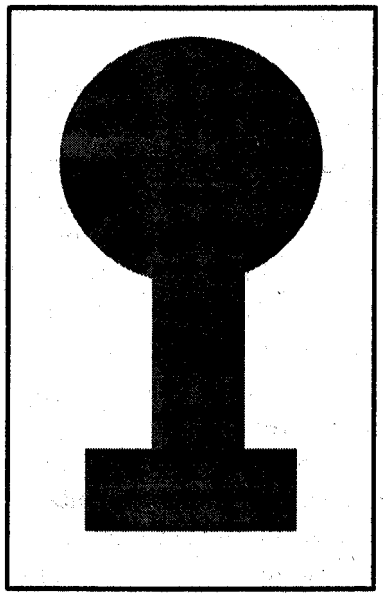

Figure 2.4: The counter electrode of the cell. The pattern is either etched in an ITO conducting plate or an aluminium coating.

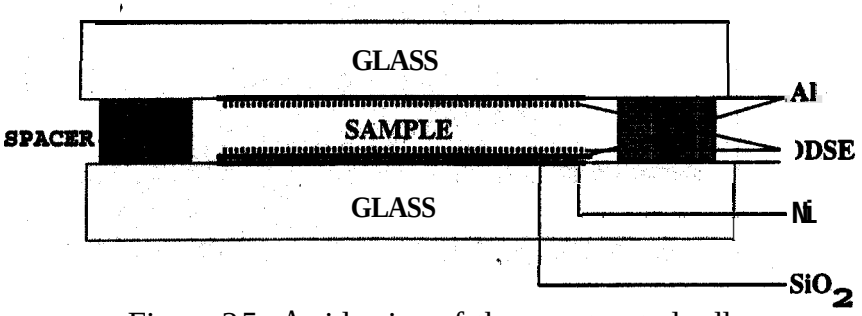

Figure 2.5: A side view of the constructed cell.

visibility of the fringes. In such cases we used a UV spectrophotometer (Hitachi) to measure the thickness of the cell, the principle being the same as explained above, except that the interference pattern is seen in transmitted light through the transparent regions around the aluminium electrode. A schematic diagram of the cross section of the assembled cell is shown in Figure 2.5. The samples were usually filled in the isotropic phase.

A four probe resistance measurement technique was used to monitor the variation of the resistance of the nickel coating as a function of temperature. As we ultimately used a 6f digit KEITHLEY (model 2000) multimeter, in principle we could measure the temperature to an accuracy of < 1mK. However the accuracy was reduced due to the limited stability of the hot stage.

2.2.2 Temperature Calibration of the Nickel Resistance Thermometer

As the resistance of the nickel film is not exactly the same in every cell due to variations in the thickness of the film, each cell is calibrated with respect to the oven temperature independently. For controlling the cell temperature we have used either a Mettler or an Instec hot stage. Initially we used a Mettler hot stage. This heater has a minimum temperature step of 0.1°C and a stability of ~ 30 mK. We used this heater without any further modifications.

As the Mettler hot stage has a large minimum temperature step and a low temperature stability, we have in later experiments replaced it with an Instec hot stage whose minimum step and maximum stability are both less than 10mK. As the position of the sensor in the HS1 hot stage is slightly below that of the sample there is a lag between the set temperature and the sample temperature depending on the rate of heating or cooling. A Minco platinum resistance thermometer (Pt RTD, 100 Ω at 0°C) calibrated (Figure 2.6) with respect to a factory calibrated unit, is fixed at a position very close to the sample. This calibration procedure was conducted to check the linearity of the platinum resistance thermometer.

As the active area of the sample was ~ 1 cm away from the Pt RTD we have calibrated the latter with respect to the sample temperature using known N-I transition points of a few compounds. These calibration runs were conducted while the sample was cooled slowly in steps of 0.05"C similar to that used in most of the experiments. Figure 2.7 shows the temperature as a function of the resistance of the Platinum thermometer. A linear function has been fitted to the data. The nickel resistance thermometer in turn is calibrated with respect to the Pt RTD. The absolute accuracy of the sample temperature, and hence the nickel resistance thermometer is 0.1°C.

The temperature stability (typically 10 to 30mk) is determined by the RMS deviation of the temperature measured by the platinum resistance thermometer. As we cannot conduct optical transmission studies, due to the opacity of the bottom electrode, we have closed the hole in

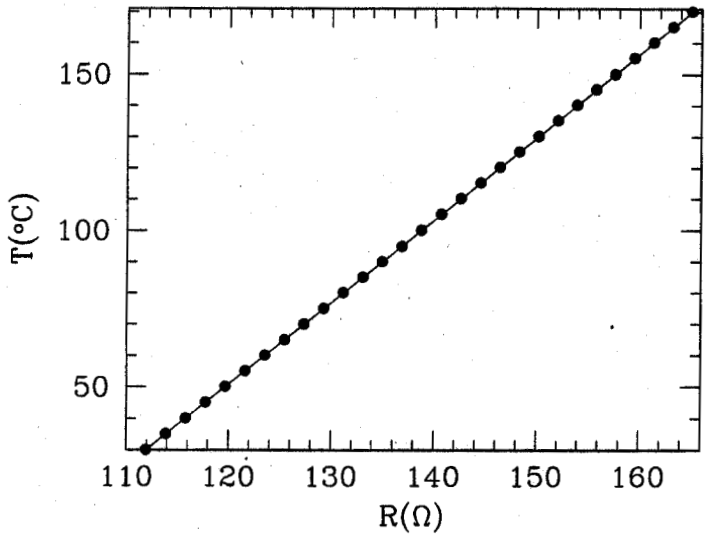

Figure **2.6:** Temperature Calibration curve for the Minco platinum resistance thermometer fixed close to the sample. The calibration is with respect to a factory calibrated platinum resistance thermometer.

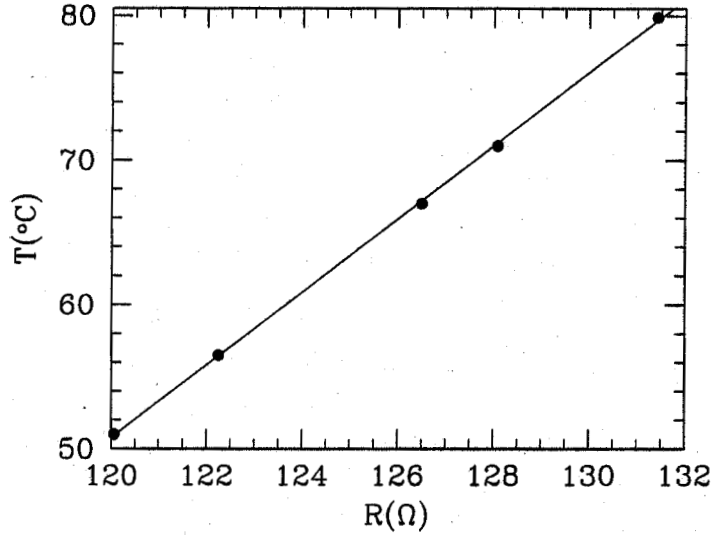

Figure **2.7:** Calibration of the temperature at the location of the sample **with** respect to the Minco platinum resistance thermometer. The points correspond to the N-I transition points of a few different nematic compounds. The equation of the fitted curve is $T=-253.034+2.531\times R$.

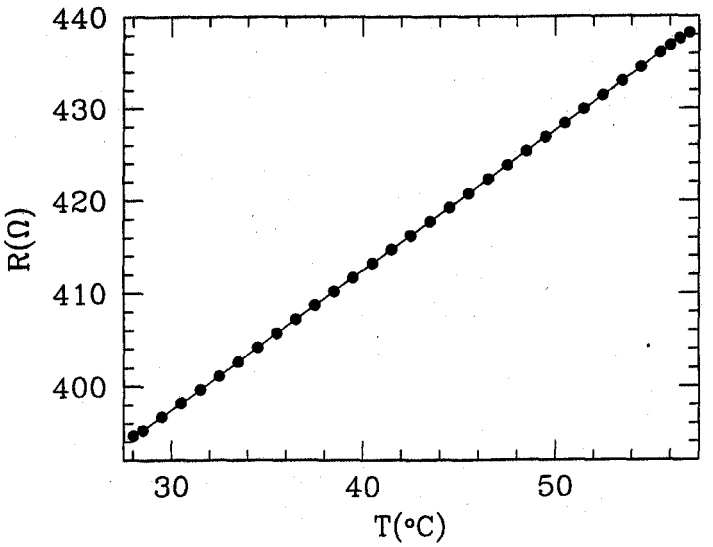

Figure 2.8: Variation of the resistance of the nickel resistance thermometer over a temperature range of $\sim 30°C$ range. The line is a guide to the eye.

the lower part of the heater using small copper blocks. This reduced the temperature gradient across the sample.

The variation of the resistance of the nickel film in one of the cells as a function of temperature is shown in Figure 2.8. Over small temperature ranges within which many of the experiments were conducted the variation is linear (Figure 2.9). It is hence sufficient to measure the resistance at two extreme temperatures, in such small ranges, and linearly interpolate for intermediate temperatures.

It was found that in some cells the resistance of the connections made to the cell varied over a period of time, i.e. the total resistance of the thermometer was not reproducible at the extreme temperature points. Such cells were discarded.

The reliability of the nickel resistance thermometer is reflected in the following experiments. A cell which was made following the above procedure was filled with octyloxy cyanobiphenyl (8OCB) and kept in a Mettler hot stage. We monitored over a period of four hours the temperature of the sample as measured by the nickel thermometer as well as the resistance of the sample itself (the details of the experimental procedure for the latter measurement will be described later in this chapter). In this experiment the sample was subjected to an RMS sinusoidal voltage of 350 V at a frequency of 250 Hz, while maintaining the Mettler temperature at $60°C$. The sample temperature and the sample resistance are shown as functions of time in Figure 2.10. After the electric field is applied, the sample temperature rises by $\sim 1.5°C$ in a few minutes, and as the heat lost through conduction in the glass plates etc is balanced by that generated by the dissipation, the temperature slowly decreases by $\sim 0.2°C$ (Figure 2.10). In addition, the slow fluctuations with magnitude $\pm 0.1°C$ in the temperature of the Mettler hot stage can also be seen in the data. The resistance of 8OCB, at the low frequency at which this experiment was conducted, is also very sensitive to temperature, decreasing as the temperature increases. Thus the resistance data shown in Figure 2.10 is almost an exact reflection of the temperature data,

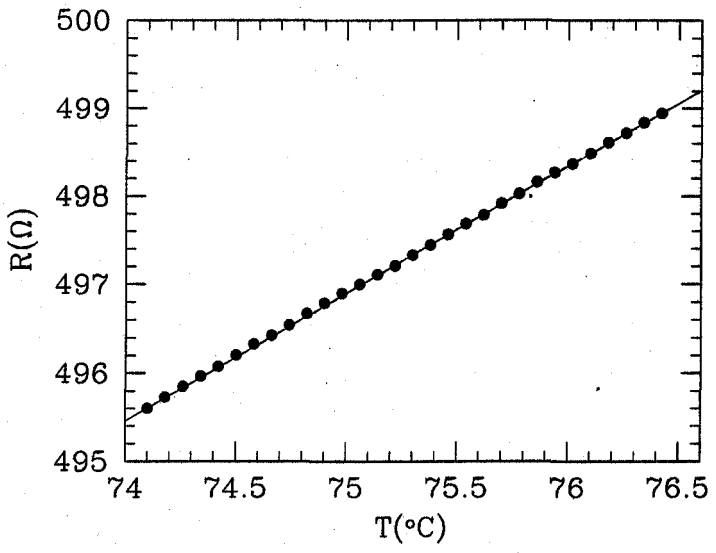

Figure **2.9:** Variation of the resistance of the nickel resistance thermometer over a temperature range of $\sim 2.5°C$ range. The line is a linear fit to the data points.

and shows that the local temperature is quite accurately measured by the nickel thermometer. Since the time constant used to measure the electrical parameters of the cell is $\leq$ **100** msec, it can be estimated that the sample temperature measurement is accurate to $\pm 0.01°C$ in this particular experiment.

Keeping the Mettler hot stage at a fixed temperature **(33.7°C),** AC voltages increasing linearly with time were applied to a pentyl cyano biphenyl **(5CB)** sample, at different frequencies. Simultaneously the local temperature was measured. It can be seen in Figure **2.11** that the local temperature increases nonlinearly with the applied voltage. Also it is higher for higher frequencies as expected, due to the dielectric heating effect.

To quantitatively study the field effect, we have used both an electrical impedance analysis of the cell and optical measurements. From the impedance analysis we measure the dielectric constant which is sensitive to the long range orientational order in the medium and also the resistance of the sample which is sensitive to the short range translational order in the medium if any.

2.2.3 Measurement of Electrical Impedance

As described in Section **2.2.1** the liquid crystal is taken between two electrodes the separation between which is controlled by mylar spacers. The capacitance of the cell increases from a value C_o in the absence of the liquid crystal to ϵC_o after filling the liquid crystal where ϵ is an appropriate dielectric constant of the material. Ideally, it would be useful to measure both $\epsilon_{\|}$ and $\epsilon_{\perp}$ as the anisotropy $(\epsilon_{\|} - \epsilon_{\perp})$ is a measure of the orientational order parameter S. For this purpose one usually applies a very small **AC** electric field to the sample such that it does not change the orientation of the director. The latter is controlled by using a magnetic field, and the same cell can be used to measure both $\epsilon_{\|}$ and $\epsilon_{\perp}$ by changing the orientation of the cell with

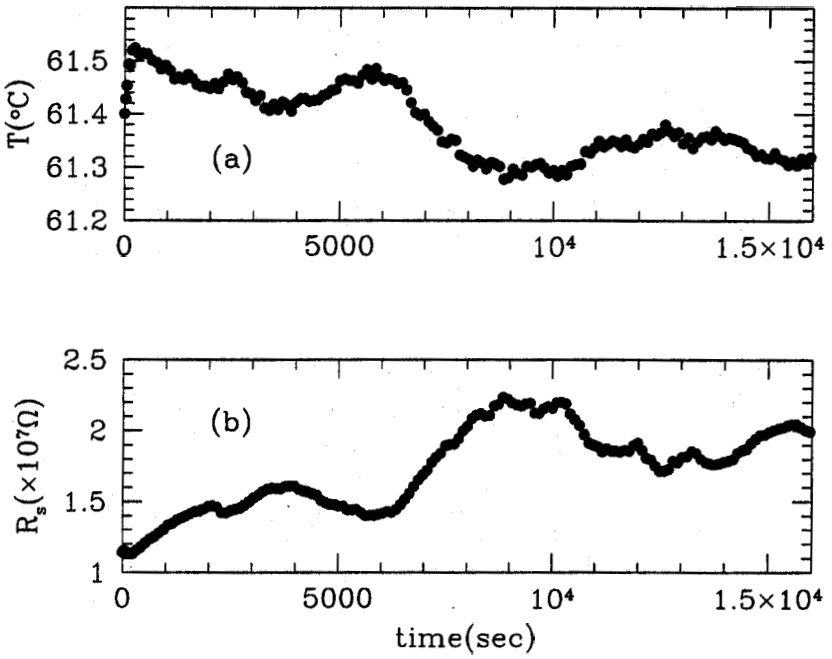

Figure 2.10: (a) The variation of the local temperature as a function of time, with a constant voltage (350 V 250 Hz) applied to a 19 pm cell filled with 8OCB.(b) The variation of the resistance of. the same sample as a function of time.

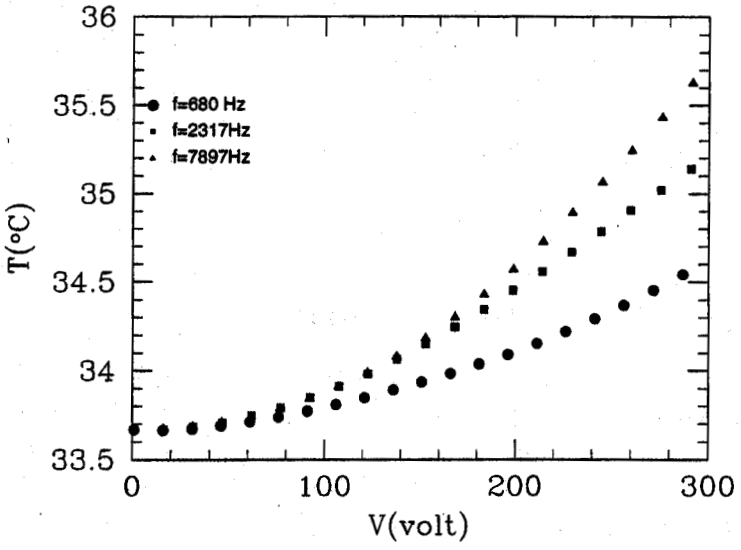

Figure 2.11: Increase in the local temperature in a 5CB sample (in the isotropic phase) as a function of the applied AC voltage at different frequencies. The oven temperature was maintained at 33.7°C. d = 19μm.

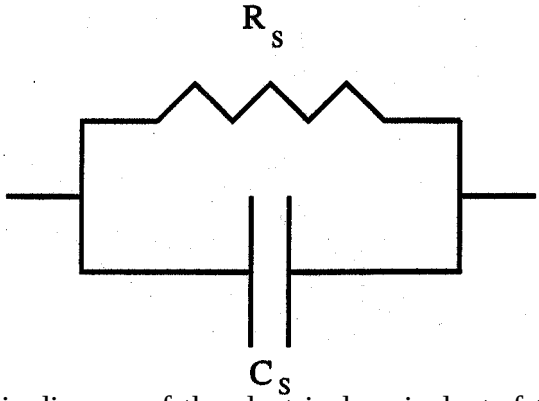

Figure 2.12: Schematic diagram of the electrical equivalent of the experimental cell.

respect to the magnetic field. However in our experiments we apply a very large electric field to the sample, and depending on the dielectric anisotropy the director will align either parallel or perpendicular to the field direction, thus making it possible to measure only one of the principal dielectric constants.

As mentioned previously liquid crystals are not free of ionic impurities, and as such they have a finite resistance. The equivalent electrical circuit of a liquid crystal cell can hence be considered to be a capacitance (C_s) and a resistance (R,) in parallel (see Figure 2.12). We measure the impedance of the sample cell and calculate its capacitance and resistance. In the experiments to be described in this thesis we have used either sinusoidal or square waveforms. The sinusoidal waveform was derived form the oscillator output of a lock-in amplifier (SRS 830), whereas the square waveform was derived from a HP synthesizer (model 3326A). The block diagram of the setup for the impedance measurement using the sine and square waveforms are shown in Figures 2.13 and 2.14.

In the experiments using a sine waveform the output of the SRS 830 lock-in amplifier (LIA) was amplified by a Trek model 601B amplifier which has a gain bandwidth of 3 MHz. The maximum output of the amplifier is 500 V and the current is limited to 10 mA. The amplifier has three similar independent units. The exact amplitude and phase of the output depends on the unit used, the frequency and amplitude of the input voltage. The output of the amplifier is applied to one of the two branches (see Figures 2.13 and 2.14), either a series resistance circuit or the sample cell in series with a capacitance C_m. A manual DPDT switch is used to switch between the two branches. The amplitude (V_o) and phase (ψ_m) of the output of the amplifier is calculated by measuring the AC signal developed across a resistance R_2(~ 100 52) in series with a large resistance $R_1 \sim 10^6$ 52. They are given by

$$V_o = v_2 \frac{R_1 + R_2}{R_2} \tag{2.11}$$

and

$$\psi_m = \phi_2 \tag{2.12}$$

where v_2 and ϕ_2 are the amplitude and phase of the signal measured across the series resistor R_2. In the experiments in which we use a square waveform, the output of the HP synthesizer is fed to the LIA before amplification as an external reference for the AC measurement. To protect the LIA from accidental high currents, (for eg if the cell shorted) two zenor diodes with their opposite polarities interconnected, as shown in Figure 2.15, are connected across the input of the LIA. The diodes have a breakdown voltage of ~ 15 V. It was found, by an independent

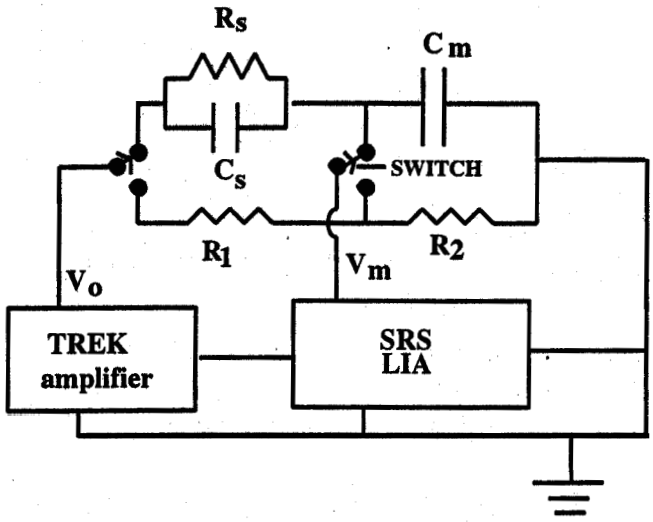

Figure 2.13: The block diagram of the setup for conducting impedance measurements using a sine wave excitation.

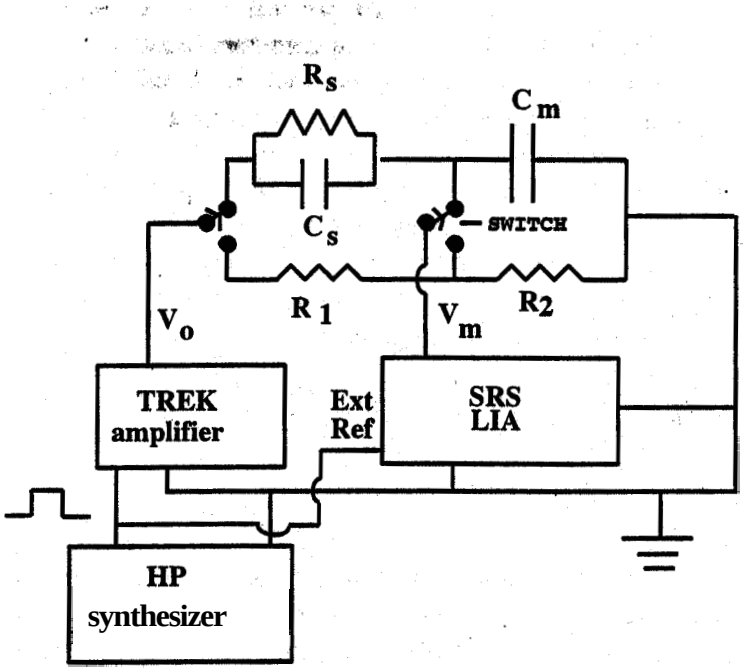

Figure 2.14: The block diagram of the setup for conducting impedance measurements using a square wave excitation.

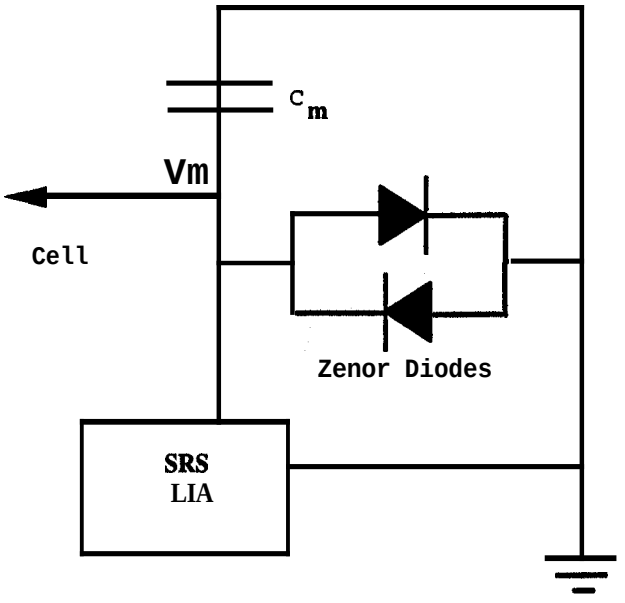

Figure 2.15: The block diagram of the zenor diode circuit connected across the measuring port of the lock in amplifier to protect it from large currents.

measurement, that this diode circuit did not change the amplitude and phase of the measured signal.

2.2.4 Impedance Analysis of the Sample Circuit.

As mentioned previously, we consider the sample cell to be the electrical equivalent of a resistor and capacitor in parallel (see Figure 2.12). We measure the amplitude and phase of the voltage developed across a series capacitance, C_m ($\sim$ 1 μFarad), which is large in comparison to the capacitance of the sample cell ($\sim$ 150 pF). It is important that C_m is large so that the maximum voltage drop is across the cell and only a small voltage is measured by the LIA. The impedance of the sample cell is given by

$$Z_c = R, \frac{(1 - i\omega C_s R_s)}{1 + \omega^2 C_s^2 R_s^2} \tag{2.13}$$

where R, is the resistance and C_s is the capacitance of the cell. $w = 2\pi f$ where f is the frequency of the applied voltage. The total impedance of the circuit (Z_t) is given by

$$Z_t = \frac{\omega R_s C_m - i(1 + \omega^2 R_s^2 C_s (C_m + C_s))}{\omega C_m (1 + \omega^2 C_s^2 R_s^2)} \tag{2.14}$$

The total current I_t, is given by

$$I_t = \frac{V_o e^{i(\omega t + \psi_m)} \omega C_m (1 + \omega^2 C_s^2 R_s^2))}{\omega R_s C_m - i(1 + \omega^2 R_s^2 C_s (C_m + C_s))}. \tag{2.15}$$

The voltage drop across C_m which is measured by the LIA is given by

$$V = V_m e^{i(\omega t + \phi_m)} = I_t Z_3 \tag{2.16}$$

where $Z_3 = 1/(-i\omega C_m)$ and V_m and ϕ_m are the amplitude and phase of the measured voltage.

$$V_m = |V| \tag{2.17}$$

$$\tan\phi_m = \frac{ImV}{ReV} \tag{2.18}$$

Simplifying the above expressions it can be shown that the sample resistance (R_s) and capacitance (C_s) are given by:

$$R_s = Y/2\pi f \sin a \tag{2.19}$$

$$C_s = X/Y \tag{2.20}$$

where $X = \cos a - Q$, $Y = (\sin^2 a + X^2)/C_m Q$, $Q = V_m/V_o$ and $a = \phi_m - \psi_m$. The dielectric constant of the sample is given by the ratio C_s/C_o where C_o is the capacitance of the empty cell measured before filling it. We used a standard capacitor and resistor connected in parallel in place of the sample cell to measure the stray capacitance added to the circuit by the cables used. It is found to be ~ 4 pF. The absolute accuracy of the measured capacitance is 1 to 2% whereas that of the resistance is $\sim 8\%$. In the experiments where we used the square waveform V_o, ψ_m and V in the above relations refer to that of the fundamental harmonic component.

2.2.5 Optical Measurements

As the lower plate is opaque, due to the aluminium and nickel coatings, it is not possible to conduct optical studies in the usual transmission mode. If the top plate is a transparent electrode it is possible to conduct optical studies in the reflection mode. For these studies the sample is mounted in a hot stage, which is itself placed on the rotating stage of a Leitz polarising microscope (model ORTHOPLAN). This model has a facility for reflection microscopy.

The optical setup is shown in Figure 2.16. A helium neon laser (ORIEL 3 mW, $\lambda = 0.633 \times 10^{-4}$ cm), is mounted on a stand with leveling screws which can be used to adjust the orientation of the laser beam. The laser beam is incident on a neutral density filter (ORIEL) to control the incident intensity. The stability of the laser beam is monitored by a reference photodiode (CENTRONICS OSD-5). The laser beam passes though a polariser and is incident on the sample in the reflection mode of the microscope. The beam passes through the transparent top plate of the cell and is reflected by the aluminium electrode on the bottom plate. This reflected beam from the cell passes through an analyser and is detected by a photodiode (CENTRONICS OSD-5 or INTEVAC INTENSIFIED PHOTODIODE). To accurately direct the beam onto the photodetector, the orientation of the sample is adjusted by using the leveling screws of a stand on which the hot stage is mounted. Usually an objective is used to focus the incident light onto the sample. In certain experiments in which we monitor the scattered light from the sample, the objective is not used. Specifically, for the light scattering experiments, we have used the INTEVAC INTENSIFIED PHOTODIODE. This has a large active cathode with a diameter of 1.8 cm, so that light scattered in a cone with an angle $\sim 1.8°$ around the reflected beam can be monitored. In these experiments we have used a PAR chopper in conjunction with the lock-in amplifier to accurately measure the scattered intensity (Figure 2.16).

We have measured the variation in the optical intensity in a homogeneously aligned 5CB sample of thickness 15 μm as a function of temperature (Figure 2.17). The temperature was lowered at a rate of 0.1°C per minute and the readings were taken at intervals of 0.1°C.

The transmitted intensity in the geometry of the experiment, through a uniformly aligned sample is given by

$$T = \sin^2 2\psi \frac{(1 - \cos\Delta\phi)}{2} \tag{2.21}$$

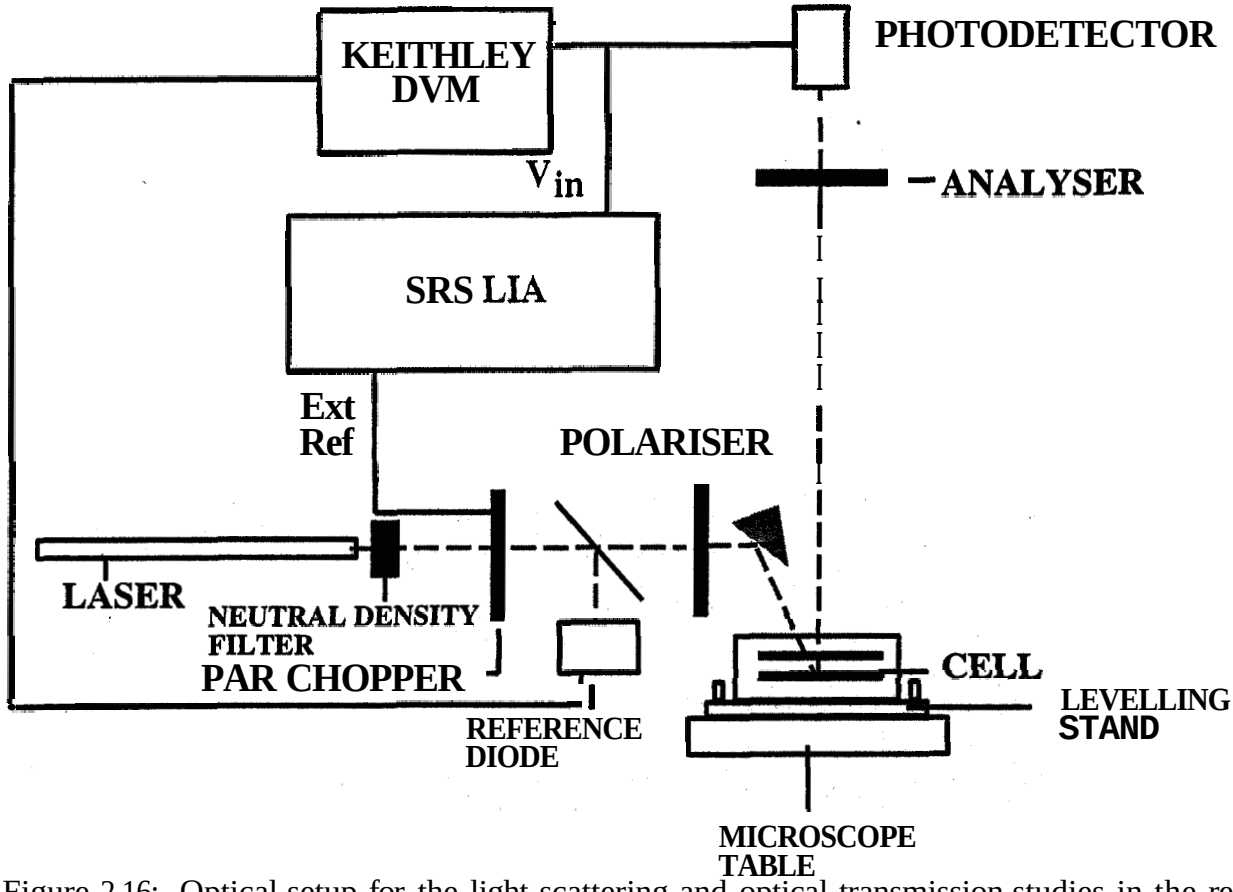

Figure 2.16: Optical setup for the light scattering and optical transmission studies in the reflection mode of the microscope. The light chopper and 'the LIA have been specifically used in the light scattering experiments. The angle of reflection from the prism and cell are highly exaggerated.for clarity.

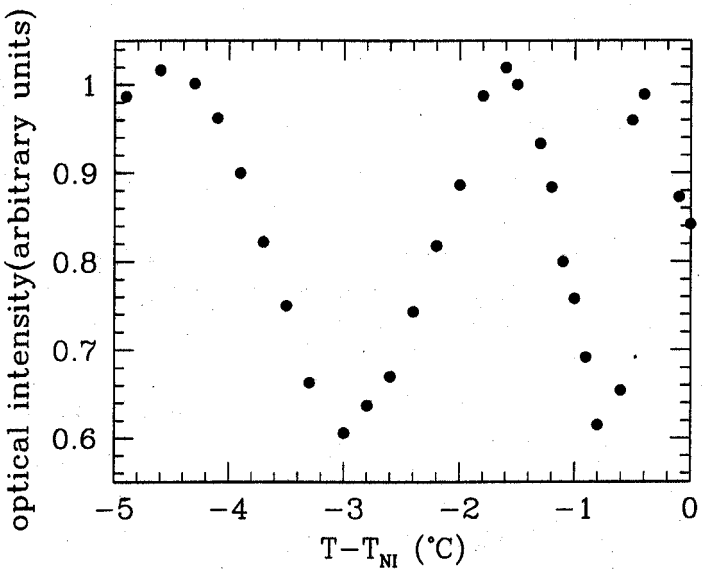

Figure 2.17: The variation of the optical signal as a function of temperature from a homogeneously aligned 5CB sample.

where T is the transmitted intensity, ψ is the angle between the director and the polariser. $\Delta\phi$ is the phase difference between the ordinary and extraordinary waves and is given by

$$\Delta\phi = \frac{2\pi}{\lambda}(n_e - n_o)2d \tag{2.22}$$

where n_o and n_e are the ordinary and extraordinary refractive indices of the liquid crystal, d is the sample thickness and λ is the wavelength of light used and the factor 2 arises from the fact that the beam passes twice through the sample. The minimum corresponds to

$$\Delta\phi = 2n\pi \tag{2.23}$$

where n is an integer. ψ is fixed at 45°. n is calculated at one temperature by using the values of n_e and n_o taken from the reference [44]. We have calculated the temperature variation of the birefringence from the data shown in Figure 2.17 and the agreement with the previous measurement is good (Figure 2.18).

2.2.6 Computer Control

The experiments were computer (AT 486) controlled by a software developed by SPECTRUM INTERFACE. As mentioned earlier in our initial experimental setup we were using the Mettler hot stage for the temperature control. We were conducting only electrical impedance measurements and using the first kind of electrode pattern without a guard ring. A block diagram of the experimental setup is shown in Figure 2.19. The nickel resistance was measured with a HP digital multimeter Model 3458A.

After replacing the Mettler hot stage with the INSTEC heater we incorporated the optical measurement in the experiment. The schematic diagram of this revised setup is shown in Figure

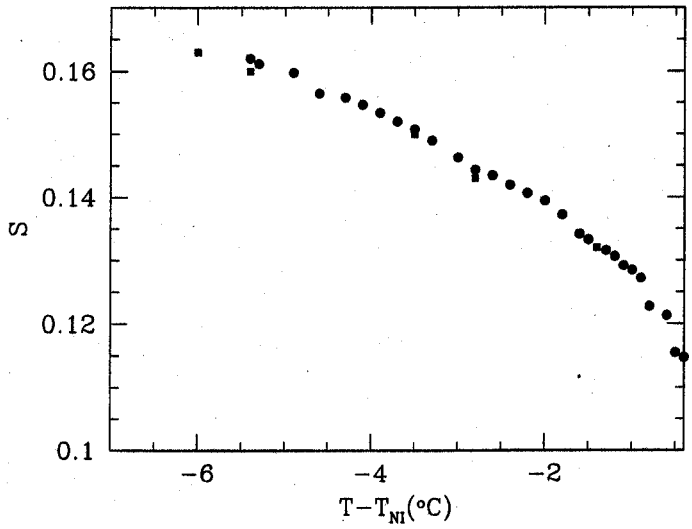

Figure **2.18:** The variation of the birefringence calculated from the data in Figure **2.17** and compared with the previous measurement. Filled circles are our measurements whereas filled squares are taken from Reference [44].

2.20. The electrode pattern has a guard ring. The nickel resistance and DC optical signals from the reference diode and the detector used to monitor the light intensity reflected from the sample are measured with a KEITHLEY multimeter.

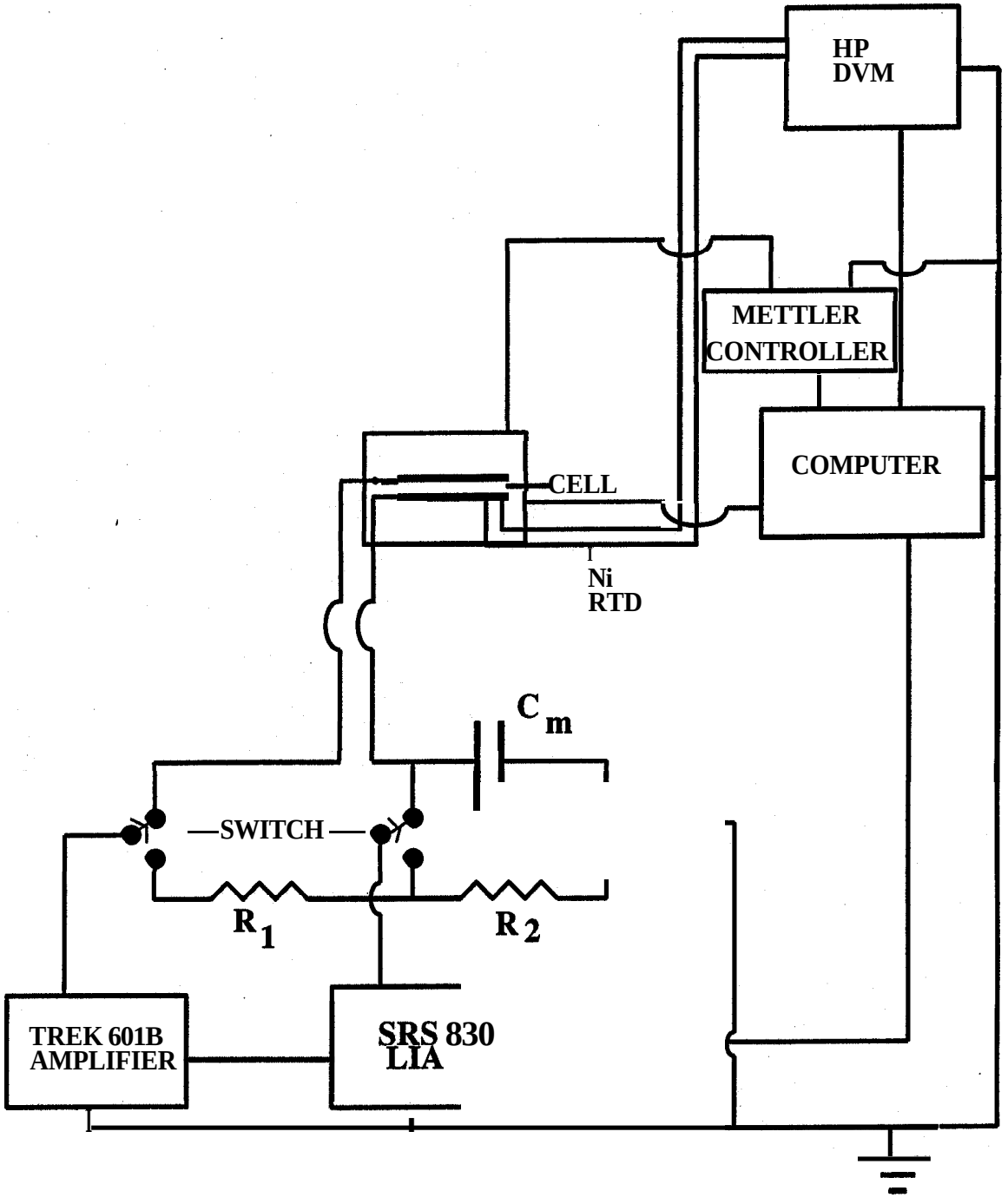

Figure 2.19: The block diagram of the initial experimental setup using the Mettler hot stage and the cell without the guard ring (sine wave excitation).

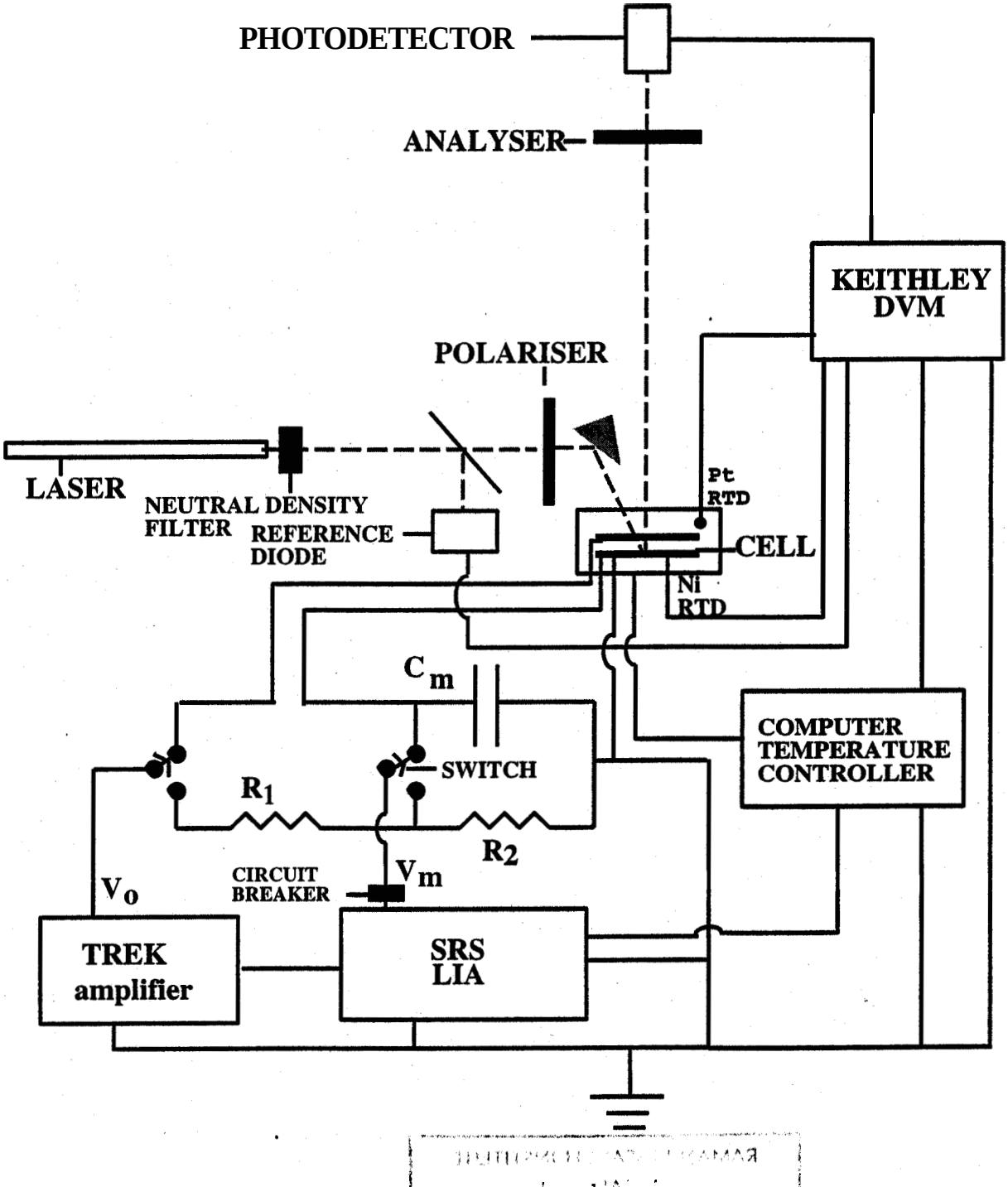

Figure 2.20: The block diagram of the improved setup using the HS1 hot stage and the cell with the guard ring using a sine wave excitation. The chopper has not been shown as it was specifically used for light scattering experiments in conjunction with the LIA as shown in Figure 2.16.